

Permanent Seismic Deformation of Highway Embankments on a Northwestern Nile Delta Profile

Mohamed F. Mansour

Geotechnical Engineering Group, Ain Shams University, Cairo, Egypt
1 El Sarayat Street, Abbasia, Cairo, Egypt, 11517

Abstract: The permanent seismic deformation of highway embankments on a typical profile encountered in the northwestern zone of Egypt's Nile delta is investigated. An artificial earthquake acceleration-time history is used to define the input seismic motion. The permanent seismic deformation is calculated by two approaches. The first approach, the Dynamic Deformation Approach (DDA), redistributes the seismic shear stresses in excess of the static shear strength in order to calculate the permanent deformation using the finite element idealization. The second approach, Newmark Approach (NA), is based on Newmark sliding block model. The results show that the permanent seismic deformation is expected to reach 100 mm, which compares well with empirical methods. The DDA rigorously accounts for the development of local yield points, while NA necessitates that the total shear stresses along a potential sliding surface are greater than the available shear strength, in order to calculate permanent deformation.

Key words: Northwestern Nile delta profile • Permanent seismic deformation • Highway embankments
• Newmark-type analysis • Earthquake geotechnics

INTRODUCTION

Earth structures suffer additional deformation due to earthquakes. The deformation may be excessive such that the serviceability of the structures is jeopardized. Several factors control the severity of the permanent seismic deformation, such as the intensity and duration of motion, the strength and stiffness of the soil materials and the liquefaction potential. The presence of liquefiable soils beneath an earth structure is a major cause of a complete collapse [1-3]. Otherwise, the resulting permanent deformation is mainly due to overstressing during the seismic excitation.

Newmark [4] developed the sliding block model that was the basis of numerous studies on the seismic displacement response of slopes. As the model was developed for infinite slopes, Chopra [5] extended the model to be capable of estimating the permanent deformation of finite slopes. Newmark sliding block model and Chopra modifications are explained. Many researchers elaborated on Newmark-type analysis and some compared it with numerical methods. You and

Michalowski [6] developed displacement charts to calculate the irreversible seismic slope toe displacement. Assuming a rotational failure mechanism, they calculated the displacements in terms of a coefficient characteristic of a given collapse mechanism (either toe failure or passing beneath the toe) and a double time integral of an earthquake acceleration record. Biondi *et al.* [7] calculated the permanent seismic displacement of infinite saturated cohesionless slopes using Newmark-type analysis and taking into account the effect of the excess pore pressure on the effective stress decrease. They found that the excess pore pressure reduces the value of the yield acceleration. Biondi *et al.* [8] extended the study to account for the occurrence of flow failure if liquefaction is approached. Zangeneh [9] proposed modifications to Newmark sliding block model to account for the seismically induced excess pore water pressure and its dissipation after the end of the earthquake.

Kim and Sitar [10] investigated the influencing factors on the seismic slope displacements using simulated acceleration-time histories. They found that the most influencing factor is the earthquake ground motion and

the seismic response is relatively less affected by the variability in the earth slope properties. Law *et al.* [11] used the finite difference method to calculate the seismically induced permanent displacements of Waba Dam in Eastern Ontario, Canada. They concluded that the permanent deformation occurred due to the formation of yield zones during the seismic excitation.

Chugh and Stark [12] calculated the permanent displacement of a relatively shallow landslide using a continuum mechanics approach and Newmark-type analysis. The results were in practical agreement since the landslide could be practically treated like an infinite slope. Bray and Travasarou [13] developed a semi-empirical probability-based model to predict the seismic deviatoric displacements of soil slopes, based on a comprehensive database from 41 earthquakes. The model was based on a nonlinear stick-slip sliding block model. The main source of uncertainty was the input ground motion. The sliding mass yield coefficient and fundamental period are the main factors affecting the seismic response of the system. The model predictions are generally consistent with documented cases of earth dam and solid-waste landfills. Garevski *et al.* [14] compared also the results of Newmark-type analysis and numerical analysis for an actual landslide and found that Newmark-type analysis overestimated the permanent slope deformations. Zhao and Song [15] developed a methodology to calculate the expected value of Newmark displacement for landslides, based on simulated acceleration-time histories. The methodology was verified by comparing the results with actual observations. Zhao and Song [15] concluded that the use of Newmark-based procedure in landslides does not deviate from realism since landslides can be reasonably approximated by an infinite slope. Kim and Sitar [16] introduced probabilistic concepts to Newmark-type analysis to account for both the material (soil) and load (earthquake) uncertainties in calculating the permanent seismic deformations. Du [17] proposed a new one-step Newmark displacement model based on seismological variables like the moment magnitude and rupture distance rather than intensity measures. The modified Newmark model by Du [17] yielded better prediction of the slope displacements.

In Egypt, the International Coastal Road (ICR) runs parallel to the Mediterranean Sea coast in the northern part of the Nile delta with offsets ranging from 350 m to more than 12 km. The prevailing soil formation consists of a succession of very soft to stiff clays and medium dense to very dense sands. The ICR embankment is constructed

on the ground surface after improving the properties of the top soft clay. Under static conditions, attention is usually drawn to the deformations associated with the clay consolidation and embankment construction.

In this paper, the permanent seismic deformation of highway embankments on a typical profile encountered in the northwestern zone of the Nile delta is estimated by numerical analysis. The typical soil profile and the highway embankment are subjected to an artificial earthquake acceleration-time history. The appropriate material properties are assigned to the different soil types. Two different approaches are used to estimate the permanent deformation. The first approach is the Dynamic Deformation Approach (DDA), which utilizes the finite element method to calculate the seismic shear stresses and compare them with the static shear strength in order to calculate the permanent seismic deformation. The second approach is Newmark Approach (NA), which is based on Newmark sliding block model and Chopra [5] modifications. The results of the two approaches are compared and the limitations are discussed.

Description of the Problem: The subsurface conditions in the northwestern Nile delta region consist typically of a top very soft to soft normally consolidated clay overlying a medium dense sand layer. The medium dense sand layer is underlain by a stiff to very stiff clay layer, which overlies a dense to very dense sand layer. Figure 1 shows a typical profile depicted in some projects very close to the ICR in the area under study. The top very soft to soft, highly plastic, silty clay layer extends to a depth of 24.0 m below the ground surface. The middle medium dense to dense sand layer has a thickness of 3.0 m and overlies the lower 7.0m-thick stiff to very stiff, highly plastic silty clay layer. The lower sand layer extends to a presumed depth of 50.0 m where the bedrock is considered to exist. The groundwater table lies at the ground surface. The results of some field and laboratory tests are shown on the soil profile in Figure 1.

The constructed ICR embankments have different heights according to the natural ground elevation and the design elevation of the highway. Embankment heights of 2.0 m and 4.0 m are investigated in this study. The embankment width is taken 30.0 m and the side slopes are taken 3H:2V. The main geotechnical engineering challenge in this profile is improving the properties of the top very soft to soft clay prior to the construction of the embankment. In many cases, the embankment is used for preloading the underlying soft clay.

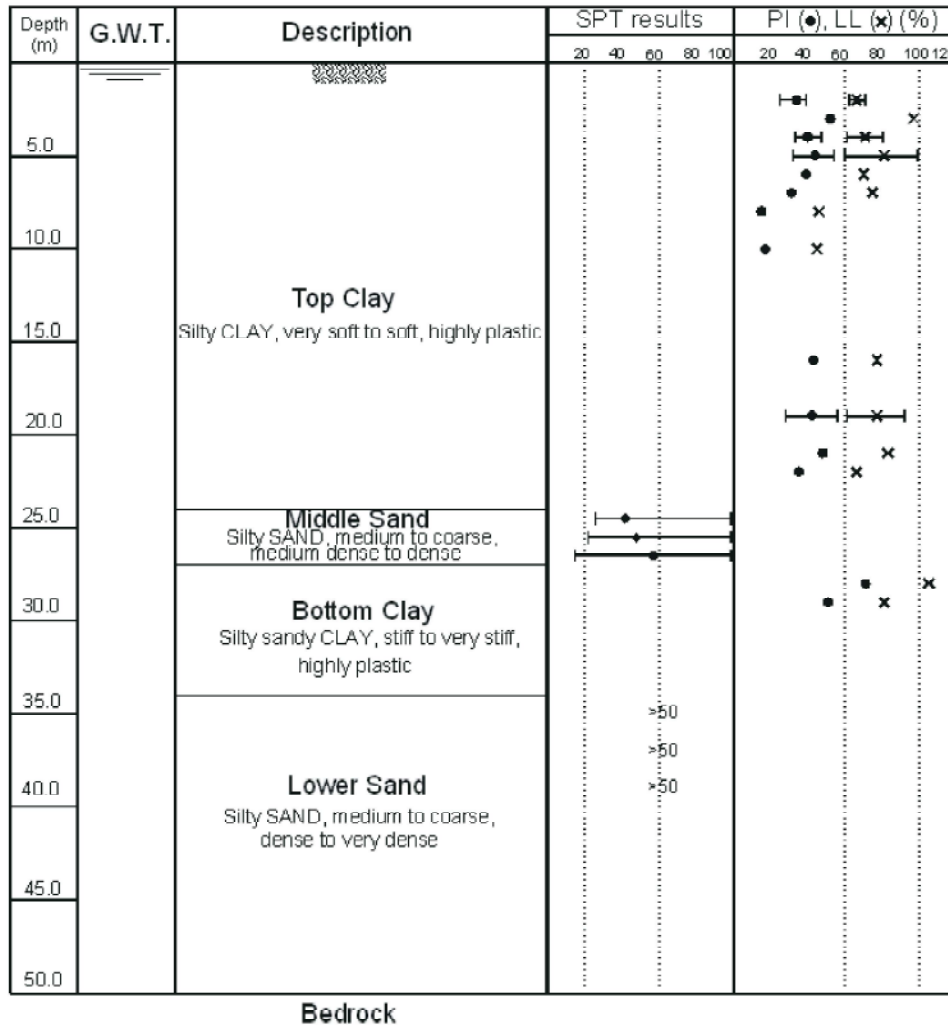


Fig. 1: Typical northwestern Nile delta profile

However, this technique may not be enough when the underlying soil strength is very low, the layer thickness is large and/or the preloading embankment height is small. Sand drains were used along some sections of the ICR to expedite the consolidation process and improve the compressibility characteristics. This study focuses on the long-term seismic behavior of highway embankments founded on the adopted soil profile. Hence, it is considered that the top clay has been improved.

MATERIALS AND METHODS

This section describes the methodologies used by the two different approaches in this study. The analysis based on the first approach (DDA) proceeds in three steps. In the first step, the long-term static conditions are

established by conducting static finite element analyses to calculate the stresses in the soil mass due to the own weight of the different soil types, the embankment weight and the live load of the moving traffic. The second step involves conducting seismic finite element analyses, where the input earthquake motion is applied at the lower boundary of the model. At each time step during the earthquake, the seismic shear stresses are calculated. The third step involves redistributing the seismic shear stresses by conducting a static finite element analysis to compare the calculated seismic shear stresses with the available static shear strength.

In the third step, the numerical model computes an incremental load vector (ΔF) based on the stress difference between two time steps. The load vector is computed for each element from:

$$\{\Delta F\} = \int_v [B]^t \{\Delta \sigma\} dv \quad (1)$$

where $\{\Delta \sigma\} = \{\sigma_n\} - \{\sigma_{n-1}\}$ is the incremental nodal stress and n is the particular time step during the earthquake, $[B]$ is the strain-displacement matrix and dv is the differential displacement.

The incremental load vector (ΔF) in Equation (1) is the algebraic difference in the stress states between two successive time steps. If the seismic shear stresses are greater than the shear strength at certain nodes, plastic points develop and, hence, the permanent seismic deformation is calculated by the numerical model. Therefore, the DDA calculates a displacement time history at each time step during the earthquake. The software GeoStudio 2007 [18,19] is used to conduct the analysis based on the DDA. Figure 2 shows the finite element meshes used in the static and seismic analyses. The mesh is relatively fine in the embankment zone and gets coarser with increasing the depth. Preliminary analyses show that the free field seismic shear stresses can be achieved with the side boundaries at a distance of 50.0 m from the toe of the embankment in both directions.

The DDA approach is compared with the classical procedure developed by Chopra [5] based on Newmark sliding block model, i.e. Newmark Approach (NA). Newmark [4] postulated that accelerations in excess of the yield acceleration can be double integrated to calculate the permanent deformation of a sliding block. The yield acceleration is the acceleration corresponding to a factor of safety of unity. Chopra [5] developed a procedure to apply Newmark approach to dams and accordingly to finite slopes. Chopra performed dynamic stress-deformation analyses and the resulting horizontal dynamic shear stresses within the potential failure surface are integrated over the potential sliding surface to obtain a resultant horizontal force at a particular time step during an earthquake. The resultant horizontal force is divided by the mass of the potential sliding wedge to obtain the average acceleration. The yield acceleration is defined by Chopra [5] as the average acceleration corresponding to a factor of safety of unity. Accelerations in excess of the yield acceleration are double integrated to calculate the permanent slope deformation. The limit equilibrium software SLOPE/W [20] is utilized to calculate the permanent deformation according to NA.

Input Motion: An artificial earthquake acceleration-time history is used to define the input earthquake motion at the lower boundary. The generated artificial time history

is based on the standard response spectrum of the Uniform Building Code (Abdel-Motaal [21]). Mokhtar *et al.* [22] found that the lateral seismic displacement of piles in liquefiable soils is slightly affected when the earthquake duration increases from 20 to 40 seconds. Hence, the earthquake duration is taken 20 seconds with 0.01 sec time interval. Figure 3 shows the acceleration-time history applied at the lower boundary. The peak horizontal acceleration is taken 0.15g to be representative of the seismic intensity in the region under study.

Constitutive Models and Material Properties: Mohr-Coulomb failure criterion is used to define the yield conditions in the different materials under static conditions; i.e. the constitutive law is elastic-perfectly plastic. The Equivalent Linear Model is used to define the degradation of the soil shear modulus with the cyclic shear strain amplitude during the seismic excitation. As described above, the seismic analysis is used to determine the seismic shear stresses that will be used as an input to subsequent static analyses to calculate the permanent seismic deformation. Therefore, it is considered that there is no need to adopt a sophisticated nonlinear dynamic model.

The material properties are based on the results of field and laboratory tests conducted for some projects in the area under study (the northwestern zone of the Nile delta). The SPT blows count and Atterberg's limits are shown in Figure 1. Mohr-Coulomb analysis requires the definition of the soil unit weight, the shear strength parameters (C and ϕ), the elastic deformation modulus (E) and Poisson's ratio (ν). The Equivalent Linear Model requires the definition of the maximum shear modulus (G_{max}) either as a constant or as a function of the in situ stress, the modulus reduction curve (variation of G/G_{max} with the cyclic shear strain amplitude, γ) and the damping ratio (ξ) either as a constant or as a function of the cyclic shear strain amplitude (γ).

The strength and deformation parameters required for the different layers are correlated with the index properties and SPT blows number shown in Figure 1, based on some well-established correlations in the literature. The top very soft to soft clay is usually improved before or during construction of the embankment, as explained above. It is considered in this study that the Top Clay has reached a medium stiff condition. The average undrained shear strength (S_u) is taken 40.0 kPa. The undrained deformation modulus (E_u) is taken $600 \cdot S_u$ according to the value of the plasticity index and over consolidation ratio (Duncan and Buchignani [23]).

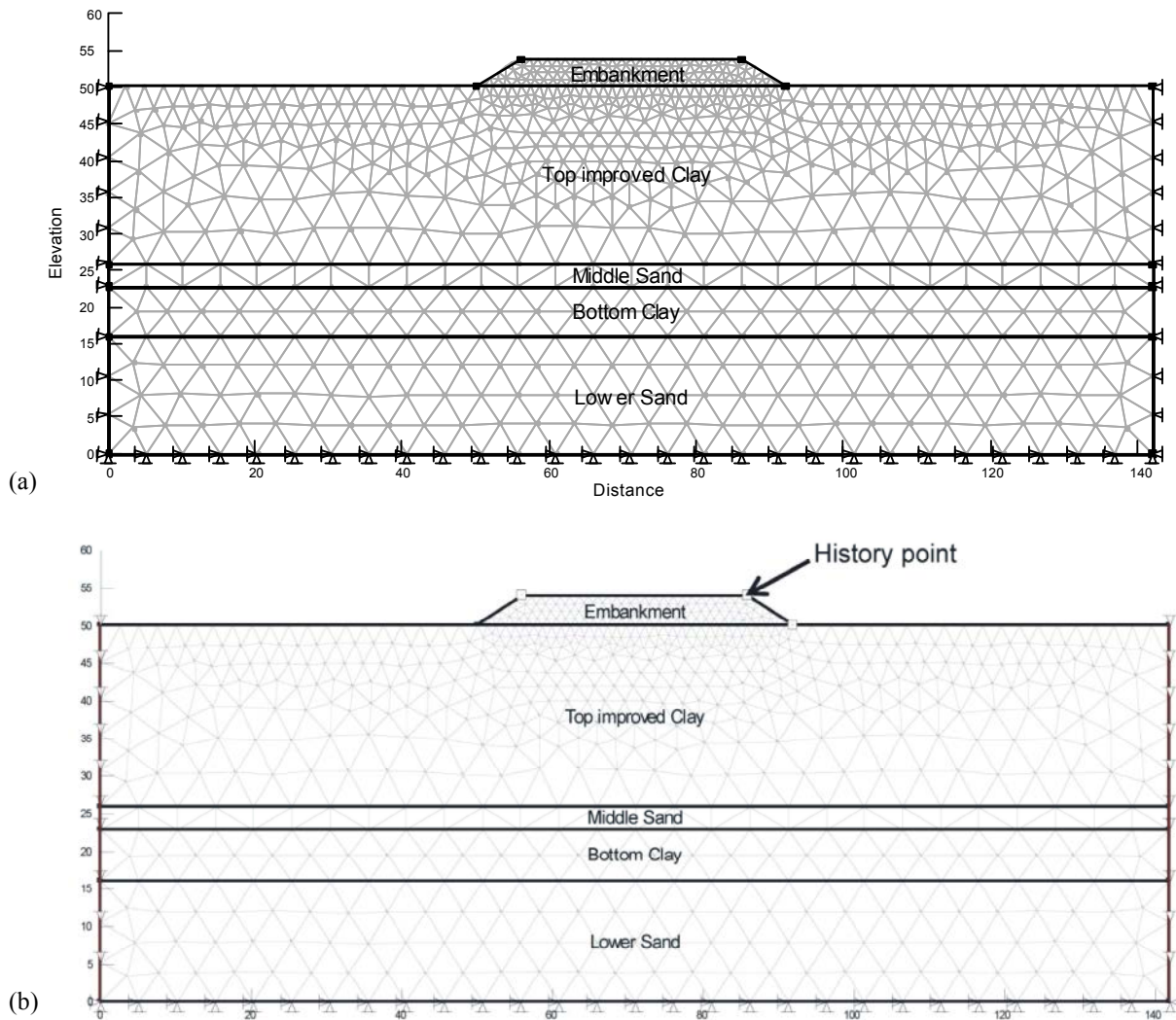


Fig. 2: Finite element mesh and boundary conditions used in: (a) static analyses and (b) dynamic analyses

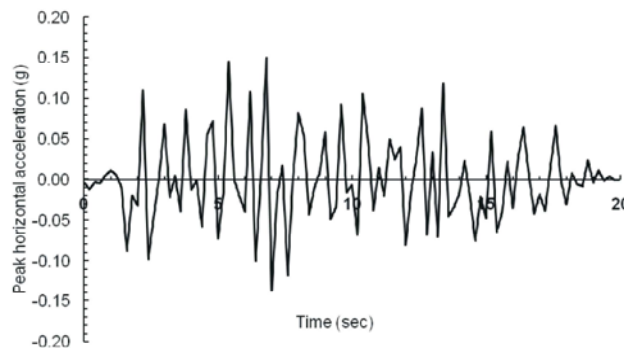


Fig. 3: Input acceleration time history

According to the elasticity theory and the values of Poisson's ratio in the undrained and drained conditions (0.50 and 0.33, respectively), the drained elastic deformation modulus of the Top Clay layer (E') is taken

$0.89 * E_u$ (by equating the undrained and drained shear moduli). Drained parameters are adopted in this study for the effective stress analysis. The drained angle of internal friction is correlated with the value of the plasticity index

(Mitchell [24]). The drained cohesion of normally consolidated clays is taken zero and is ignored for the bottom, likely overconsolidated, clay due to its little impact on the dynamic soil properties. The maximum shear modulus (G_{max}) of the Top Clay layer is estimated based on the value of the elastic deformation modulus (E') and Poisson's ratio (ν) according to the elasticity theory, as follows:

$$G = \frac{E}{2 * (1 + \nu)} \quad (2)$$

Similarly, the static strength and deformation parameters of the Bottom Clay layer are estimated. The bottom clay is stiff and, hence, the undrained shear strength (S_u) is taken 100 kPa. The undrained elastic deformation modulus (E_u) is taken $500 * S_u$ (Duncan and Buchignani [23]).

The static parameters of the Middle Sand and the Lower Sand are derived from the SPT results. As shown in Figure 1, there is a refusal to the sampler penetration in the Lower Sand layer. The internal friction angle is taken 36° . The SPT results in the Middle Sand layer indicated a dense to very dense condition with few SPT values smaller than 30. Conservatively, the value of the internal friction angle is taken 32° . The secant modulus at 50% of the failure stress (E_{50}) for the Middle Sand and Lower Sand layers varies with the confining stress according to the following equation (Schanz *et al.* [25]):

$$E_{50} = E_{ref} \cdot \left(\frac{\sigma'_3}{p_{ref}} \right)^m \quad (3)$$

where;

σ'_3 is the effective confining pressure, which equals the at rest earth pressure coefficient (K_o) times the effective vertical stress (σ'_v). K_o is taken equal to $\frac{\nu}{1-\nu}$

according to the elasticity theory,

p_{ref} is the reference pressure, taken 100 kPa,

m is a stress exponent and equals 0.5 for cohesionless soils (Janbu [26]) and

E_{ref} is the modulus corresponding to the reference pressure.

The maximum shear modulus of the Middle Sand and Lower Sand layers is calculated from Seed and Idriss [27] correlation, as shown in Equation (4).

$$G_{max} = 1000 * K_{2,max} * (\sigma'_m)^{0.5} \quad (4)$$

where;

G_{max} is the maximum shear modulus in units of lb/ft²

$K_{2,max}$ is a unitless factor that depends on the value of the relative density and

σ'_m is the mean principal stress ($\frac{\sigma'_v + 2 * K_0 * \sigma'_v}{3}$) in lb/ft².

The value of $K_{2,max}$ is taken 59, 40 and 52 for the Embankment, Middle Sand layer and Lower Sand, respectively.

The variations of the modulus reduction factor (G/G_{max}) and damping ratio (ξ) with the cyclic shear strain amplitude (γ) are estimated according to the correlations developed by Ishibashi and Zhang [28]. The main advantage of these correlations is the consideration of the effects of the mean principal stress and plasticity index on the modulus reduction factor and damping ratio. The sand layers have zero plasticity indexes. For the clay layers, a plasticity index of 30% conservatively accounts for the degradation of the shear modulus with the cyclic shear strain amplitude.

Table 1 summarizes the static and dynamic parameters assigned for the different materials. Figure 4 and Figure 5 show the variations of the modulus reduction factor and damping ratio with the cyclic shear strain amplitude.

Pore Water Pressure (PWP) Functions: The generated pore pressure during seismic events causes a shear strength drop due to the effective stress decrease. This issue is primarily encountered in loose cohesionless soils, which may completely liquefy. Dense sands, on the other side, dilate rather than contract with continued cyclic shearing and, hence, there is no risk of shear strength drop during seismic events. Medium dense sands may experience an increase in pore pressure that may not cause complete liquefaction, but may cause additional deformation by virtue of the effective stress drop. The relationship between the pore pressure ratio (r_u) and the Cyclic Number Ratio (N/N_L) is defined in the numerical analysis according to the equation developed by Lee and Albaisa [29] and DeAlba *et al.* [30], as follows:

$$r_u = \frac{1}{2} + \frac{1}{\pi} \sin^{-1} \left[2 \left(\frac{N}{N_L} \right)^{1/\alpha} - 1 \right] \quad (5)$$

where r_u is the pore pressure ratio, N is the equivalent number of uniform cycles for the earthquake under study, N_L is the number of loading cycles that will cause liquefaction under a particular set of stress conditions and α is an exponent taken 0.7.

Table 1: Static and dynamic parameters used in the analysis

Material type	Unit weight (kN/m ³)	Friction angle ϕ' (°)	Undrained Modulus E_u (MPa)	Reference deformation Modulus E_{ref} (MPa)	Maximum shear modulus G_{max} (Mpa)
Embankment	19.0	36.0	NA	100.0*	See Equation (4)
Top improved Clay	18.0	28.7	24.0	21.0	8.0
Middle Sand	18.0	32.0	NA	50.0*	See Equation (4)
Bottom Clay	18.0	28.7	50.0	44.0	16.0
Lower Sand	18.0	36.0	NA	120.0*	See Equation (4)

*At a reference confining stress of 100.0 kPa.

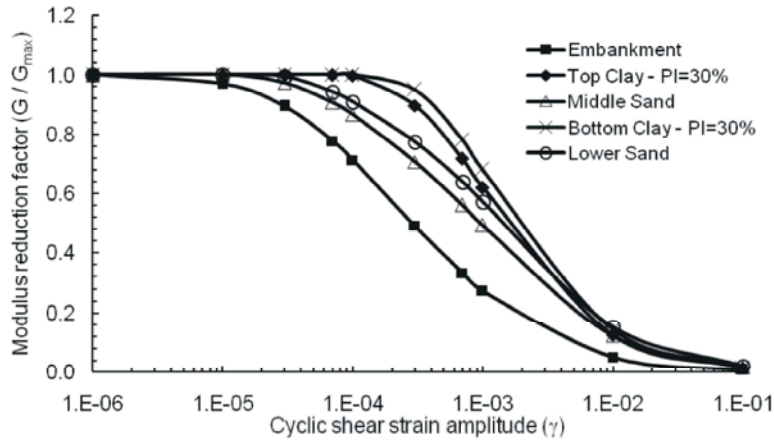


Fig. 4: Variation of the modulus reduction factor (G/G_{max}) with the cyclic shear strain amplitude (γ)

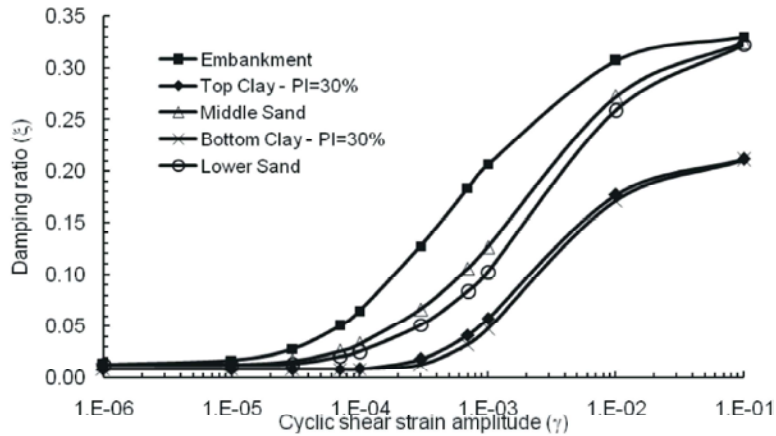


Fig. 5: Variation of the damping ratio (ξ) with the cyclic shear strain amplitude (γ)

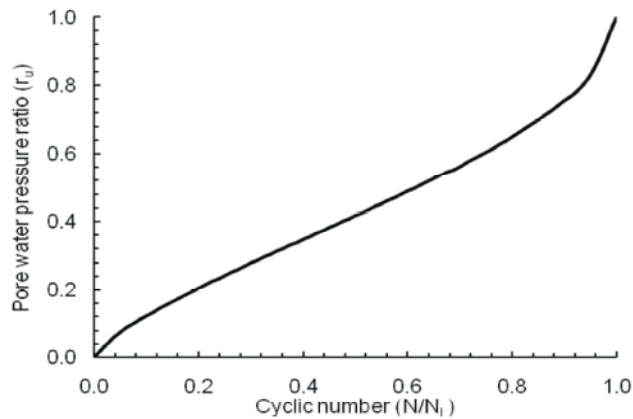


Fig. 6: Pore water pressure ratio (r_u) as a function of the cyclic number (N/N_L) for the Middle Sand layer

The Lower Sand layer is in a dense to very dense condition, based on the SPT results. Therefore, no PWP function is defined for the Lower Sand layer. The Middle Sand layer is generally dense with SPT blows number greater than 30. Four SPT recordings were smaller than 30 and one value was equal to 15. The numerical analyses are conducted with a PWP function for the Middle Sand layer only.

The equivalent number of loading cycles (N) is determined from the charts developed by Seed *et al.* [31] considering the earthquake magnitude (taken 7.0) and a cyclic shear stress amplitude of 0.65 times the peak shear stress. The number of loading cycles required to produce initial liquefaction (N_L) is determined based on the results published by Seed and Lee [32]. Their results for the medium dense case are used in this study. Figure 6 shows the estimated PWP function for the Middle Sand layer.

RESULTS

As pointed out above, two approaches are used in this study. In the first approach, the permanent deformation is calculated by conducting a post-earthquake static analysis using the seismically induced shear stresses. This approach is referred to as the Dynamic Deformation Approach (DDA). In the second approach, the permanent deformation is estimated based on the approach developed by Chopra [5] based on Newmark sliding block model. This approach is referred to as Newmark Approach (NA).

Results of the Dynamic Deformation Approach (DDA)

Analysis: The results are interpreted in terms of the following:

- The variation with time of the embankment crest displacement and
- The acceleration-time history at the embankment crest

Figure 7 shows the vertical displacement time history of the left and right crests of the 2m high embankment. The maximum vertical displacement of 21 mm is encountered at the right crest. The excess PWP contours in the Middle Sand layer are shown in Figure 8. The excess PWP is less than 2.0 kPa, which indicates a negligible effect on the overall deformation. Therefore, the calculated permanent deformation is mainly due to overstressing during the seismic excitation.

Figure 9 shows the horizontal displacement time history of the left and right crests of the 2m high embankment. The right crest suffers also higher horizontal displacement than the left crest. The peak value equals 82 mm at the time of about 15.6 sec. The corresponding vertical displacement at the same duration equals 20 mm. The resultant displacement equals 84 mm. Figure 10 shows the deformed mesh of the 2m high embankment after the end of the earthquake episode.

Figure 11 shows the vertical displacement time history of the 4m high embankment left and right crests. The maximum vertical displacement of the right crest is increased to 38 mm, i.e. by 80%. The excess PWP is also smaller than 2kPa. Figure 12 shows the horizontal displacement time history. The peak horizontal displacement reaches 96 mm at 15.6 sec. The corresponding horizontal displacement equals 36 mm. Therefore, the total displacement equals 103 mm. The deformation pattern is similar to the 2m high embankment.

The above results indicate that highway embankments constructed on the profile under study are expected to deform by about 100mm during seismic excitation. From the serviceability point of view, it is important to check the differential movements between different points along the embankment. Figure 13 shows the calculated vertical displacement (settlement) troughs for the cases of the 2m and 4m high embankments. The middle point of the embankment settles by a very small value relative to the left and right crests. This behavior is apparently attributed to the lack of confinement near the embankment side slopes relative to the middle part. Therefore, the calculated total vertical displacement can be considered equal to the differential settlement of the highway embankment; i.e. the differential settlement may reach 37 mm. Figure 14 shows the differential horizontal deformation of the left and right crests of the 2m and 4m high embankments. The differential horizontal deformation equals 20 mm and 25 mm for the 2m and 4m high embankments, respectively.

The results are also viewed from the standpoint of the acceleration response at the top of the embankment. Figure 15 shows the acceleration response of the right crest of the 2m and 4m high embankments. Both responses are essentially similar, owed to the very small difference between the total depths of the two models (52 m and 54 m, respectively). Figure 15 shows that the peak crest acceleration reaches 0.186g. The seismic waves are propagated through stronger cohesionless soils and relatively weaker cohesive soils. The results show that the overall effect of the soil profile is a 24% magnification of the input motion.

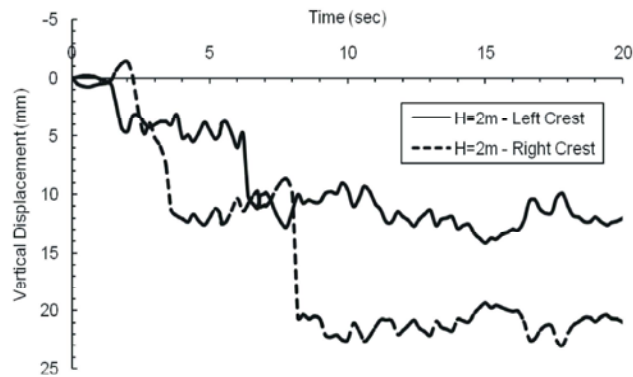


Fig. 7: Vertical displacement of the 2m-high embankment crest

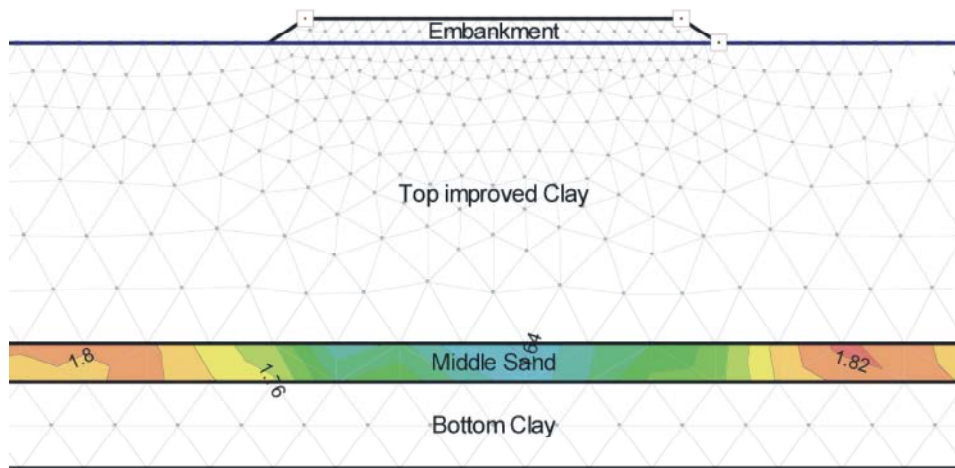


Fig. 8: Excess pore water pressure (PWP) in the Middle Sand layer for the case of 2m-high embankment

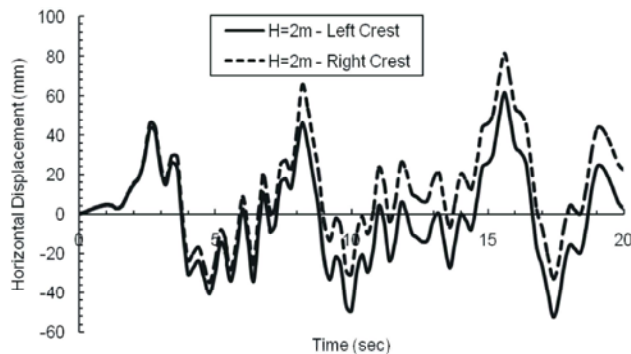


Fig. 9: Horizontal displacement of the 2m-high embankment crest

Results of Newmark Approach (NA) Analysis: The output of the seismic analysis is used to run a limit equilibrium analysis based on the methodology developed by Chopra [5], which is described in Section 7. As the analysis is solved per time step, the results are interpreted as a plot of the factor of safety versus time. Figure 16 shows the factor of safety versus time for the 2m and 4m high embankments. Figure 17 shows the factor

of safety against average acceleration for the 2m and 4m high embankments. The results show that the factor of safety does not drop below unity. Hence, according to Newmark model and Chopra modifications, the yield acceleration is higher than the maximum average acceleration that occurred during the seismic excitation. Accordingly, Newmark-type analysis predicts zero permanent deformation for the embankment under study.

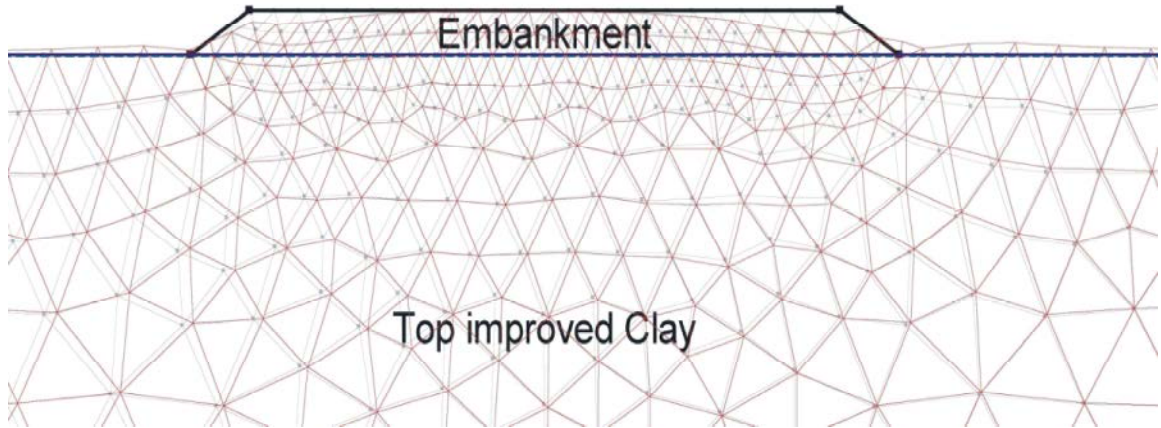


Fig. 10: Deformed mesh of the 2m-high embankment (exaggeration = 40X)

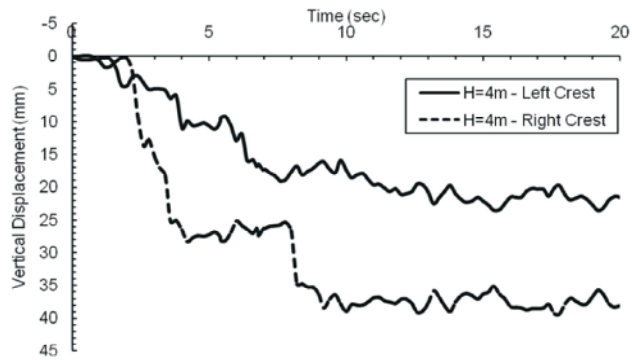


Fig. 11: Vertical displacement of the 4m-high embankment crest

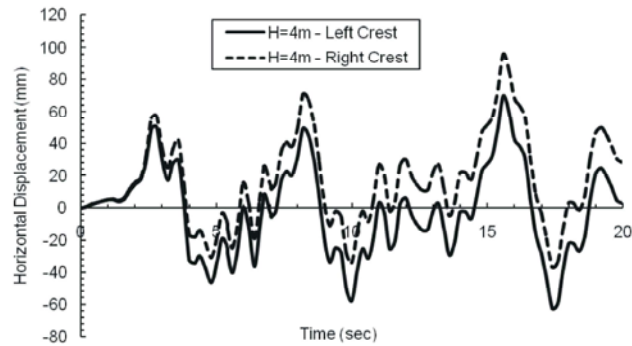


Fig. 12: Horizontal displacement of the 4m-high embankment crest

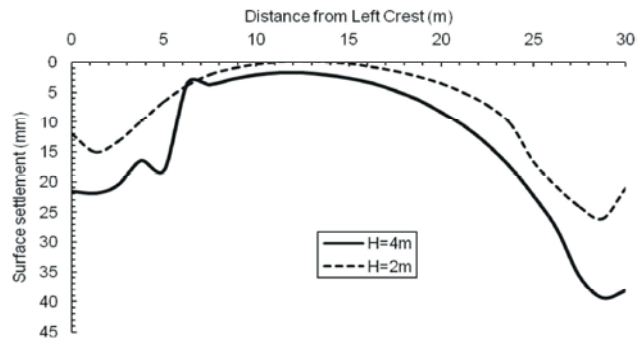


Fig. 13: Settlement trough of the 2m and 4m-high embankments

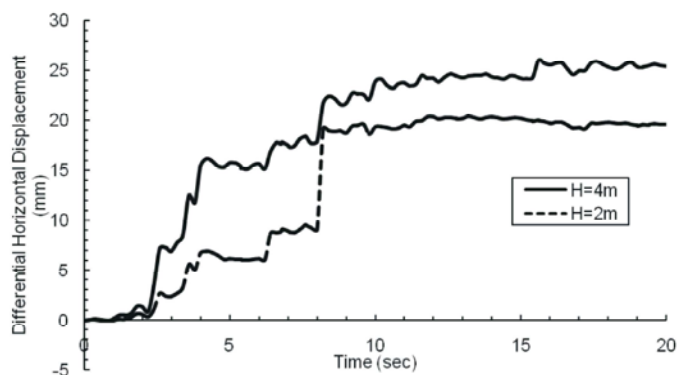


Fig. 14: Differential horizontal displacement of the left and right crests

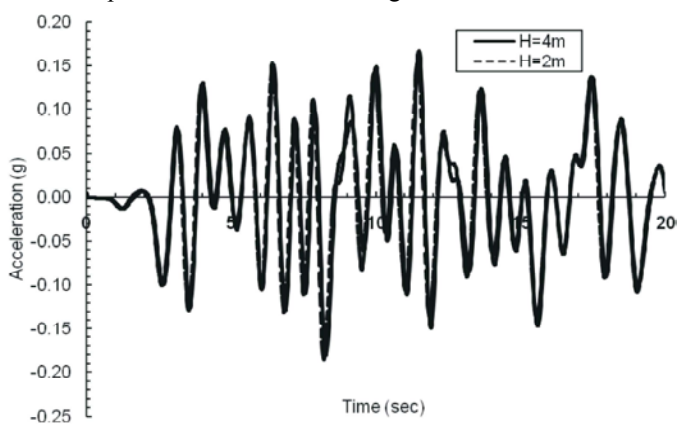


Fig. 15: Acceleration response at the right crest of the 2m and 4m-high embankments

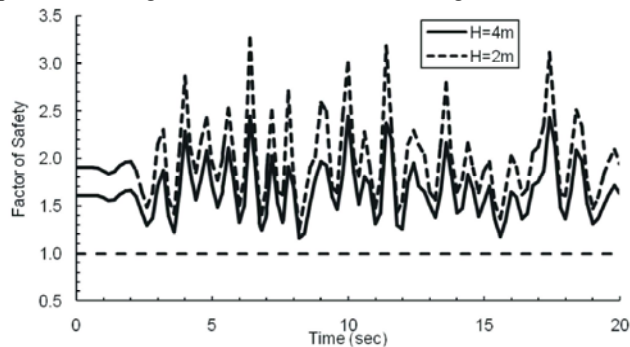


Fig. 16: Factor of safety versus time for the 2m and 4m-high embankments

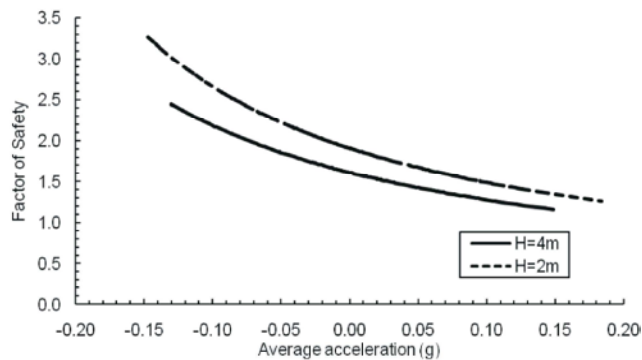


Fig. 17: Factor of safety versus average acceleration for the 2m and 4m-high embankment slopes

DISCUSSION

This paper presents the results of a numerical study using two approaches to calculate the permanent seismic deformation of embankments resting on a typical soil profile encountered in the northwestern zone of the Nile delta. The two approaches seem to be in complete disagreement with respect to calculating the permanent seismic deformation. The difference is mainly attributed to the concept used in calculating the slope deformation. The first approach, the DDA, calculates the seismically induced shear stresses at each node at each time step during the earthquake. Static finite element analyses are used to calculate the permanent seismic deformation based on the adopted yield criterion (Mohr-Coulomb). Therefore, according to this approach, it is not a requisite to reach complete yielding everywhere inside the slope to obtain permanent deformation. The calculated deformation of the embankment is the accumulation of the deformation resulting from local yielding at different nodes.

On the other side, the second approach (NA) is, in essence, a limit equilibrium approach. It necessitates that the total shear stresses along a potential sliding surface become greater than the soil shear strength for a permanent deformation to develop, i.e. the concept of a “global factor of safety”. As long as the total shear stresses along a potential sliding surface are less than the soil shear strength, no deformation occurs according to NA.

Therefore, the DDA is considered a rigorous approach to estimate the permanent seismic deformation of embankment slopes, since it accounts for the local yielding at every single node of the finite element mesh. The resulting crest deformation is the accumulation of the displacement occurring at all the yielding nodes along the profile. Newmark approach does not account for local yielding either across the whole mesh or within the potential sliding mass.

This study shows that highway embankments constructed on the studied profile are expected to deform by up to 100 mm during a 20-second long earthquake with a peak ground acceleration of 0.15g. The excess pore pressures are very low and their impact on the deformation is negligible. The deformation values could have been much larger if any of the investigated materials is liquefiable.

These results are based on estimated material properties/functions from well-established correlations in

the literature. Extensive laboratory tests and field monitoring during and after earthquakes will help to verify and enhance the numerical model. Although there are no field measurements to support the results of this study, the results compare well with the empirical equation developed by Swaisgood [33]. Swaisgood calculated the embankment crest settlement (ΔH), given that no liquefaction occurs, as a function of the peak ground acceleration (PGA), the surface wave magnitude (M_s) and the summation of the embankment and foundation soil heights (H), as shown in Equation (6).

$$\frac{\Delta H}{H} (\%) = e^{(6.07PGA + 0.57M_s - 8.0)} \quad (6)$$

The calculated crest settlements of the 2m and 4m high embankments, 21 mm and 38 mm, respectively, can be reproduced from Equation (6) for surface wave magnitudes of 6.4 and 7.5, respectively. This comparison shows that the implemented model is capable of predicting the embankment deformation within the same order of magnitude of Equation (6).

Pells and Fell [34] developed a damage classification system where the damage class is related to the maximum longitudinal crack width and the maximum relative crest settlement. The 2m and 4m high embankments investigated in this study experience relative crest settlements of 26mm and 37mm, respectively, i.e. 0.05% and 0.07 % of the total studied heights (52 m and 54 m, respectively). The corresponding damage class is “Minor” and the expected maximum longitudinal crack width according to Pells and Fell [34] ranges from 10 mm to 30 mm. The calculated differential horizontal deformations in this study equal 25 mm and 37 mm, i.e. close to the values predicted by Pells and Fell [34].

CONCLUSIONS

Finite element and limit equilibrium analyses are conducted on a typical soil profile encountered in the northwestern zone of the Nile delta, in order to estimate the permanent seismic deformation of highway embankments. The conclusions of the study can be summarized in the following points:

- The expected permanent seismic deformation of highway embankment slopes on the studied profile may reach 100 mm.

- The differential movement may reach 37 mm in the vertical direction and 25 mm in the horizontal direction. These values need to be considered in the seismic design of the highway. The calculated values compare well with empirical correlations from the literature. However, field monitoring and dynamic laboratory testing can improve the reliability of the results.
- The presence of subsurface liquefiable soils is expected to cause a significant increase in the calculated deformation.
- The two implemented approaches are significantly different on the conceptual level. The classical Newmark Approach adopts the concept of a “global factor of safety” where the total shear stresses along a potential sliding surface need to be higher than the available shear strength to cause permanent deformation.
- The Dynamic Deformation Approach is a powerful tool to estimate the permanent seismic deformation, as it accounts for the development of local yield zones and calculates the resulting deformation accordingly.
- The characteristics of the soil materials in the studied profile cause an overall magnification of about 24% of the input peak horizontal acceleration.

REFERENCES

1. Bhatnagar, S., S. Kumari and V. Sawant, 2015. Numerical analysis of earth embankment resting on liquefiable soil and remedial measures. *International Journal of Geomechanics*. DOI: [http://dx.doi.org/10.1061/\(ASCE\)GM.1943-5622.0000501](http://dx.doi.org/10.1061/(ASCE)GM.1943-5622.0000501).
2. Huang, Y., A. Yashima, K. Sawada and F. Zhang, 2009. A case study of seismic response of earth embankment foundation on liquefiable soils. *Journal of Central South University of Technology*, 16(6): 994-1000.
3. Adalier, K. and M.K. Sharp, 2004. Dynamic behavior of embankment dam on liquefiable foundation subject to moderate earthquake loading. 13th World Conference on Earthquake Engineering, Vancouver, BC, Canada. Paper no. 1025.
4. Newmark, N.M., 1965. Effects of earthquakes on dams and embankments. *Géotechnique*, 15(2): 139-160.
5. Chopra, A.K., 1966. Earthquake effects on dams. Ph.D. thesis, University of California, Berkeley.
6. You, L. and R.L. Michalowski, 1999. Displacement charts for slopes subjected to seismic loads. *Computers and Geotechnics*, 25(1): 45-55.
7. Biondi, G., E. Cascone, M. Maugeri and E. Motta, 2000. Seismic response of saturated cohesionless slopes. *Soil Dynamics and Earthquake Engineering*, 20(1-4): 209-215.
8. Biondi, G., E. Cascone and M. Maugeri, 2002. Flow and deformation failure of sandy slopes. *Soil Dynamics and Earthquake Engineering*, 22(9-12): 1103-1114.
9. Zangeneh, N., 2003. Enhanced Newmark method for seismic analysis of submarine slopes. M. Eng. Report, Memorial University of Newfoundland, Canada.
10. Kim, J. and N. Sitar, 2003. Importance of spatial and temporal variability in the analysis of seismically-induced slope deformation. In the Proceedings of 9th International Conference on Applications of Statistics and Probability in Civil Engineering, San Francisco, pp: 1315-1322.
11. Law, K.T., K. Refahi, P. Ko, T. Lam and P. Hassan, 2005. Seismic Deformation of Waba Dam. Conference Proceeding: Canadian Dam Association, Calgary, Canada.
12. Chugh, A.K. and T.D. Stark, 2006. Permanent seismic deformation analysis of a landslide. *Landslides*, 3: 2-12.
13. Bray, J.D. and T. Travasarou, 2007. Simplified procedure for estimating earthquake-induced deviatoric slope displacements. *Journal of Geotechnical and Geo-environmental Engineering*, 133(4): 381-392.
14. Garevski, M., Z. Zucig and V. Sesov, 2013. Advanced seismic slope stability analysis. *Landslides*, 10(6): 729-736.
15. Zhao, H. and E. Song, 2012. A method for predicting co-seismic displacements of slopes for landslide hazard zonation. *Soil Dynamics and Earthquake Engineering*, 40: 62-77.
16. Kim, J.M. and N. Sitar, 2013. Probabilistic evaluation of seismically induced permanent deformation of slopes. *Soil Dynamics and Earthquake Engineering*, 44: 67-77.
17. Du, W., 2013. Earthquake-induced slope displacement analysis using spatially-correlated vector intensity measures. Ph.D. Thesis, Hong Kong University of Science and Technology.

18. GEO-SLOPE International Ltd. 2008. Stress-Deformation Modeling with SIGMA/W 2007, Third Edition.
19. GEO-SLOPE International Ltd. 2008. Dynamic Modeling with QUAKE/W 2007, Third Edition.
20. GEO-SLOPE International Ltd. 2008. Stability Modeling with SLOPE/W 2007, Third Edition.
21. Abdel-Motaal, M.A., 1999. Soil effect on the dynamic behavior of framed structures. Ph.D. Thesis, Ain Shams University, Egypt.
22. Mokhtar, A.A., M.A. Abdel-Motaal and M.M. Wahidy, 2014. Lateral displacement and pile instability due to soil liquefaction using numerical model. *Ain Shams Engineering J.*, 5(4): 1019-1032.
23. Duncan, J.M. and A.L. Buchignani, 1976. An Engineering Manual for Settlement Studies. Department of Civil Engineering, University of California, Berkeley, pp: 94.
24. Mitchell, J.K., 1976. Fundamentals of Soil Behavior, John Wiley and Sons, New York, pp: 422.
25. Schanz, T., P.A. Vermeer and P.G. Bonnier, 1999. Formulation and verification of the Hardening-Soil model. In R.B.J. Brinkgreve, *Beyond 2000 in Computational Geotechnica*, Balkema, Rotterdam, pp: 281-290.
26. Janbu, J., 1963. Soil compressibility as determined by Oedometer and triaxial tests. In *Proceedings of 3rd European Conference on Soil Mechanics and Foundation Engineering*, Wiesbaden, Germany, pp: 19-25.
27. Seed, H.B. and I.M. Idriss, 1970. Soil moduli and damping factors for dynamic response analyses. Report EERC 70-10, Earthquake Engineering Research Center, University of California, Berkeley.
28. Ishibashi, I. and X. Zhang, 1993. Unified dynamic shear moduli and damping ratios of sand and clay. *Soils and Foundations*, 33(1): 182-191.
29. Lee, K.L. and A. Albaisa, 1974. Earthquake Induced Settlements in Saturated Sands. *Journal of the Geotechnical Engineering Division, ASCE*, 100(GT4): 387-406.
30. DeAlba, P., C.K. Chan and H.B. Seed, 1975. Determination of Soil Liquefaction Characteristics by Large-Scale Laboratory Tests. Report EERC 75-14, Earthquake Engineering Research Center, University of California, Berkeley.
31. Seed, H.B., K. Mori and C.K. Chan, 1975. Influence of Seismic History on the Liquefaction Characteristics of Sands. Report EERC 75-25, Earthquake Engineering Research Center, University of California, Berkeley.
32. Seed, H.B. and K.L. Lee, 1965. Studies of liquefaction of sand under cyclic loading conditions. Report TE-65-65, Department of Civil Engineering, University of California, Berkeley.
33. Swaisgood, J.R., 2003. Embankment dam deformations caused by earthquakes. In the *Proceedings of 2003 Pacific Conference on Earthquake Engineering*, Christchurch, New Zealand, Paper no. 14.
34. Pells, S. and R. Fell, 2003. Damage and cracking of embankment dams by earthquake and the implications for internal erosion and piping. In *Proceedings of the 21st International Congress on Large Dams (ICOLD)*, Montreal, Canada.